INTERNATIONAL JOURNAL FOR NUMERICAL METHODS IN FLUIDS, VOL. 7, 465–488 (1987)

THREE-DIMENSIONAL SURFACE WATER MODELLING USING A MESH ADAPTIVE TECHNIQUE

S. SARRAF*

Civil Engineering Department, Concordia University, Montreal, Canada

AND

R. KAHAWITA† AND R. CAMARERO‡

Ecole Polytechnique, Montreal, Canada

SUMMARY

Numerical simulation of open water flow in natural courses seems to be doomed to one- or two-dimensional numerical simulations. Investigations of flow hydrodynamics through the application of three-dimensional models actually have very few appearances in the literature. This paper discusses the development and the initial implementation of a general three-dimensional and time-dependent finite volume approach to simulate the hydrodynamics of surface water flow in rivers and lakes. The slightly modified Navier–Stokes equations, together with the continuity and the water depth equations, form the theoretical basis of the model. A body-fitted time-dependent co-ordinate system has been used in the solution process, in order to accommodate the commonly complex and irregular boundary and bathymetry of natural water courses. The proposed adaptive technique allows the mesh to follow the movement of the water boundaries, including the unsteady free-water surface.

The primitive variable equations are written in conservative form in the Cartesian co-ordinate system, and the computational procedure is executed in the moveable curvilinear co-ordinate system. Special stabilizing techniques are introduced in order to eliminate the oscillating behaviour associated with the finite volume formulation. Also, a new and comprehensive approximation for the pressure forces at the faces of a control volume is presented. Finally, results of several tests demonstrate the performance of the finite volume approach coupled with the adaptive technique employed in the three-dimensional time-dependent mesh system.

KEY WORDS Free Surface Flow Curvilinear Co-ordinates Three-dimensional Finite volume Mesh adaptive technique

INTRODUCTION

Since its inception, the field of computational hydraulics has concentrated on one- and later on two-dimensional modelling of open water flow. However, continuing advances in computer technology and numerical techniques will increasingly generate more interest in the modelling of more complex three-dimensional problems. Yet, the degree of success achieved in this field can

* Assistant Professor
† Professeur titulaire, dept. génie civil
‡ Professeur titulaire, dept. Math. App.

0271–2091/87/050465–24$12.00

Received 19 February 1986
Revised 18 September 1986

hardly be rated as moderate.[1,2] This is due to inherent difficulties associated with the physical characteristics of open water problems which can be summarized as follows:

1. Open water modelling deals normally with a huge body of moving water over a particularly large distance that is normally measured in kilometres. Such a physical constraint imposes severe requirements on the implementation of any particular computational scheme. It also affects the accuracy of the results, specially for three-dimensional cases, where the ratio of the vertical grid increment to the horizontal one is significantly small.

2. The condition of free surface, under which open water flows, is one, if not the most, intricate problem that three-dimensional simulation has to deal with. Complexities arise not only because the free water surface is an unsteady boundary but also from the fact that its gradients are the main factors that generate flows and induce currents. The numerical integration should be extended up to the current location of the free surface which is an unknown variable at the moment of integration. This requires special considerations in the numerical scheme. One common practice extensively used in the literature[3–5] consists of assuming a known average water surface level around which an additional function $\eta(x, t)$ describes the fluctuations in the water surface. This procedure would only harm the predictive character of the model in cases where the average water surface is unknown, and it is obviously restricted to small fluctuations.

3. Water flow encountered in natural courses is normally confined to particularly complex geometry and bathymetry that may induce complications in the local flow pattern and generate secondary currents. Therefore, this additional physical constraint has to be fully considered together with the previous two in order to ensure a minimal proper simulation. Unfortunately, instead of fitting the boundary or using interpolation to fix the cell values adjacent to the boundary, the common practice in computational hydraulics[6,7] is to replace the boundary with a completely different set of scaled lines (Figure 1). Although, in principle, a grid refinement can be used to alleviate many of these problems, the necessary degree of refinement is often totally impractical for engineering purposes.

Leendertse *et al.*[8] have devised what could be considered the first attempt to model three-dimensional circulation in open water flow. The model is based on a system of horizontal layers in which water surface fluctuations are reserved solely to the upper layer. All subsequent attempts[3–5] differ little from the above model. They mostly make use of a Cartesian co-ordinate system and a rigid-lid approximation at the free surface boundary. Later Sengupta *et al.*[9] presented a model that avoids the drawback of rigid-lid approximation while keeping most of the characters of the other models.

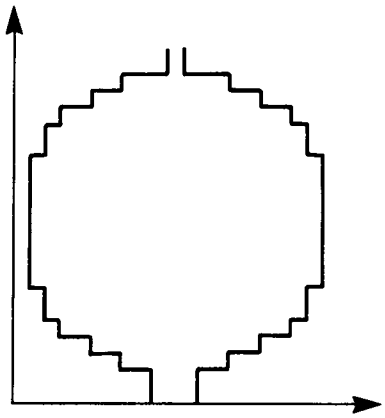

Figure 1. A circular basin computational boundary[7]

The material presented herein deals with the application of time-dependent curvilinear co-ordinates in the modelling of open water flow. These co-ordinates are used to fit the irregular boundary of the water body and to continuously track the movement of the unsteady free water surface. Therefore, the need for a rigid-lid approximation is eliminated and a more realistic approach has resulted that can adequately model the effects of the variations of the water surface as well as of the solid boundaries.

MATHEMATICAL FORMULATION

A slightly modified version of the Navier–Stokes equations forms the theoretical basis of the model. Together with the continuity and other complementary equations, they are written in a conservative form in a Cartesian co-ordinate system. Basic assumptions of homogeneous, incompressible and viscous flow are considered. A first-order turbulent closure model is used. This is based on an analogy with laminar diffusion terms applied to the eddy transport coefficients. Isotropic eddy conditions are considered in the planar direction, whereas a different value is used in the vertical direction.

The equations of motion can be written as follows:

$$(u_i)_i = 0, \qquad i = 1,2,3, \tag{1a}$$

$$(u_i)_t + (u_i u_j)_j + 2\varepsilon_{ijk}\omega_j u_k = -\frac{1}{\rho}(P)_i + g_r\delta_{3i} + [\nu_j(u_i)_j]_j, \quad i = 1,2, \quad j = 1,2,3, \tag{1b}$$

$$(P)_i - \rho g_r \delta_{ii} = 0, \qquad i = 3, \tag{1c}$$

in which $i = 1,2$, $j = 1,2,3$ are repeating indices that indicate summation, $(—)_t$ represents the derivative with respect to time, $(—)_j$ represents the derivative with respect to the jth Cartesian co-ordinate x^j, u_i are the Cartesian components of the velocity vector, t is time, g_r is the acceleration due to gravity, P is pressure, ρ is density, ν_j are the eddy viscosity coefficients, ω_j are the Cartesian components of the earth rotation vector and ε_{ijk}, δ_{ij} are the Christoffel and Kronecker symbols, respectively.

Equation (1a) governs the conservation of mass of an incompressible fluid; equation (1b) represents the momentum conservation in the eastward and northward directions, respectively; equation (1c) is the simplified form of the momentum equation in the vertical direction resulting from the application of the hydrostatic approximation. The latter consists of neglecting the vertical component of the acceleration while retaining the vertical component of the velocity throughout the computation process. This approximation is not only suggested by the physical behaviour of the flow but is also required to alleviate the high distortion of the ratio between vertical and horizontal grid increments.

Extending the hydrostatic approximation to equation (1b) gives

$$(u_i)_t + (u_i u_j)_j + 2\varepsilon_{ijk}\omega_j u_k = -g_r[(h + x_b^3) - x^3]_i + [\nu_j(u_i)_j]_j, \quad i = 1,2, \quad j = 1,2,3, \tag{2}$$

in which x^3 is the elevation of the local element with respect to a horizontal datum and x_b represents the elevation of the stream bottom with respect to the same datum.

Since equation (1c) does not contain u_3 and equation (2) includes a new variable h, two additional equations must be provided in order to evaluate these variables (i.e. h and u_3). These equations are based on special integrations of the continuity equation. The bottom shear stresses are expressed according to the quadratic shear stress law using the tangential components of the velocity adjacent to the bottom. Stresses inside the water body are accounted for through the eddy diffusion terms.

FINITE VOLUME FORMULATION

In developing computational methods for simulating flow fields in arbitrary domains, there are two basic approaches: either (1) solving the governing equations in the physical space of the flow where the discretization is based on an integral form of the Cartesian equations over an arbitrary control volume, or (2) transforming the equation as well as the computational region into a new space where the domain becomes a simple rectangular form in order to avoid the difficulty associated with specification of boundary conditions. In this work, however, the first approach is considered. Hence the Cartesian equations are integrated over a typical control volume made up of constant co-ordinate surfaces forming a non-orthogonal grid system (Figure 2).

The advantages of using the finite volume formulation numerically to compute the conservation laws lie in its ability to represent the physical phenomena in different terms rather than dealing abstractly with governing equations. This formulation is always conservative since fluxes introduced at cell boundaries are the same between two neighbouring cells. The major disadvantages of the finite volume formulation reside in the fact that it belongs to the class of central difference schemes. These are neutrally stable and generate oscillations in the computed solution.[10,11]

The grid

Fitting the water body with a three-dimensional boundary-conforming grid is further complicated by the presence of the free water surface. Although solid boundaries can also vary as a result of flooding or tide reversal, the movement of the free surface is of greater importance. Hence, it has to be accurately modelled. Continuously tracking the movement of the water surface and correctly locating its instantaneous position will be partially solved by a judicious composition of a time-dependent boundary-conforming grid. This is based on a three-dimensional curvilinear co-ordinate transformation defined as follows:

$$(T)\begin{cases} \xi_i = \xi_i(x^i, t) \\ \xi_3 = \alpha(x^3)[x^3 - x_d^3(x^i)]/h(x^i, t), \quad i = 1, 2, \\ \tau = t \end{cases} \tag{3}$$

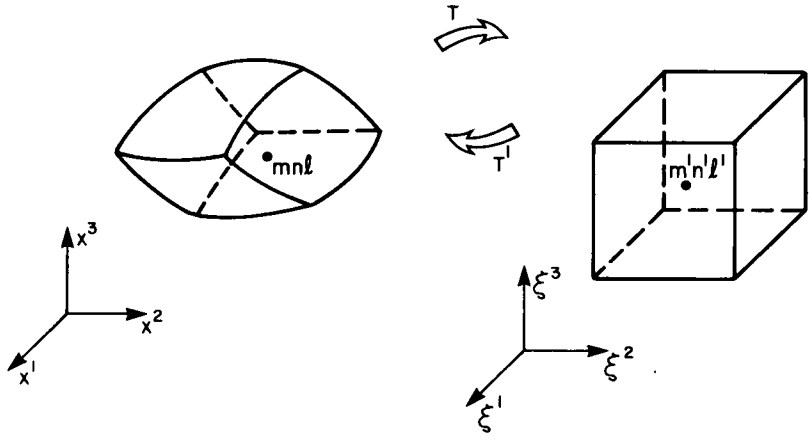

Figure 2. A curvilinear control volume and its transformed image

where (ξ_i) are the covariant components of the curvilinear co-ordinate system, x_d^3 is the vertical location of the flow bottom, α is a concentration function used to stretch the grid in the vertical direction and all other variables are as defined earlier. The inverse Jacobian of this transformation is given by

$$J^{-1} = (\xi_i)_i = [(\xi_1)_1(\xi_2)_2 - (\xi_1)_2(\xi_2)_1] \tag{4}$$

and the metric matrix is $G = JJ^{-1}$.

This co-ordinate system can be viewed as a planar two-dimensional system of ξ_1 and ξ_2 extended to three dimensions by ξ_3, which is defined separately and independently. The basic idea behind this set-up is to couple an independently defined two-dimensional bank-conforming grid to a naturally adapted system of moveable layers distributed over the depth of the water. By varying ξ_3 in the interval $[0, \alpha]$, the entire water depth can be swept accordingly. The free water surface and the stream bottom form two particular co-ordinate surfaces, designated by $\xi_3 = 0$ and $\xi_3 = \alpha$, respectively (Figure 3).

This particular formulation of the curvilinear transformation is designed chiefly to accommodate the hydraulic and topographical features pertinent to open water flow in natural courses. In fact, the free water surface as well as the bottom have considerable importance in the theory and practice of classical open channel hydraulics. Moreover, this transformation helps reduce the complexity of the mathematical derivations and integrations required by the application of the computational procedure.

The initial construction of the grid system is first made for the planar two-dimensional set by applying the method advocated by Thompson *et al.*[12] This considers the physical plane to be defined as the solution of a Laplace or Poisson equation. Grid points are arbitrarily specified on the boundaries. The generated mesh is not necessarily orthogonal, which is not a requirement to carry on numerical calculations. Once this step is accomplished ξ_3 can be subsequently incorporated. Stretching the co-ordinate lines to accommodate boundary or local requirements in the planar set can be accomplished by a special procedure outlined in Reference 12. However, the packing and refinement of the vertically distributed layers is performed by assigning appropriate functions, such as trigonometrics or polynomials, to the variable α present in the definition of ξ_3.

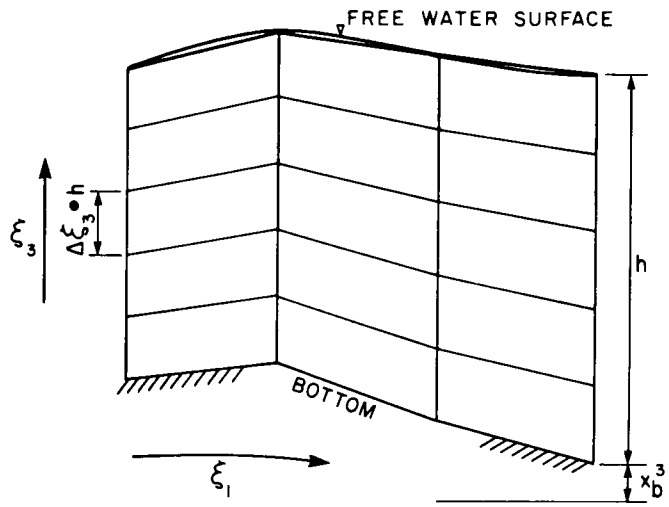

Figure 3. A vertical pack of the automatically adjusted layers

The grid system, being moveable, requires redefinition at each time step. The analytical expression of ξ_3 ensures this requirement in the vertical direction. However, relocation of the grid setting in the planar directions is directly related to the movement of the planar boundaries of the water body. The instantaneous position of a mesh node can be given then by a first-order Taylor series expansion, such as

$$x^i_{(\tau+\Delta t)} = x^i_{(\tau)} + \frac{\partial x^i_{(\tau)}}{\partial \tau} d\tau, \quad i = 1,2, \tag{5}$$

or, in terms of curvilinear co-ordinates,

$$\xi_{(t+\Delta t)} = \xi_{i(t)} + \frac{\mathbf{V}^* \cdot \boldsymbol{\xi}_i}{\sqrt{g_i}} dt, \tag{6}$$

with $\mathbf{V}^* = (x^i)_t$, $i = 1,2$ and g_i a diagonal element of the metric matrix G.

Integral formulation in moveable grids

Equations (1a) and (2) are integrated over a control volume element made of the curvilinear grid described above (Figure 4). The integration procedure is designed to evaluate an overall balance over the control volume. In order to estimate the influx and outflux, the volume integral is converted into a surface integral using Gauss's theorem. Further, owing to the variability or the movement of the control volume, Reynolds' theorem has to be applied simultaneously. The integral form of the momentum equation can be written as

$$\iiint_{V(t)} \left\{ (u_i)_t + (u_i u_j)_j + \frac{1}{\rho}(P)_i - [\nu_j (u_i)_j]_j \right\} dV = 0, \quad i = 1,2, \quad j = 1,2,3, \tag{7a}$$

$$\iiint_{V(t)} [(P)_i - \rho g_r \delta_{i3}] \, dV = 0, \quad i = 3. \tag{7b}$$

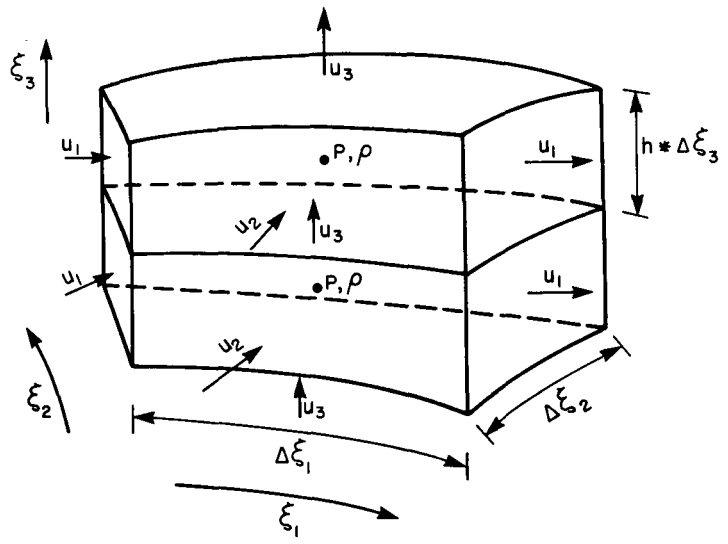

Figure 4. Location of various hydrodynamic properties on the control volume

Coriolis acceleration and body force components in the planar directions are omitted since no loss of generality would be inflicted. The application of Gauss's theorem at a fixed moment in time results in

$$\iiint_{V(t)} (u_i)_t \, dV + \iint_{S(t)} \left[u_i u_j + \frac{P}{\rho} \delta_{ij} - v_j (u_i)_j \right]_S dS_j = 0, \quad i = 1,2, \quad j = 1,2,3, \tag{8a}$$

$$\iint_{S(t)} (P - \rho g)_S \delta_{j3} \, dS_j = 0, \quad i = 3. \tag{8b}$$

$(\ )_S$ indicates that variables inside the parentheses are calculated at the face of the control volume. The application of Reynolds' transport theorem over the control volume, which is considered as a deformable medium, can result in

$$\left(\iiint_{V(\tau)} u_i \right)_\tau dV + \iint_{S(\tau)} \left[u_i u_j + \frac{P}{\rho} \delta_{ij} - u_i \tilde{u}_j - v_j (u_i)_j \right]_S dS_j = 0, \quad i = 1,2, \quad j = 1,2,3. \tag{9}$$

The additional terms ($\tilde{u}_j$) represent the Cartesian components of the intrinsic velocity of the control volume computed at the control volume faces. These are a result of the application of Reynolds' theorem which states

$$\iiint_{V(t)} [(u_i)_t] \, dV = \left(\iiint_{V(t)} u_i \right)_\tau dV + \iint_{S(t)} (\tilde{u}_i u_j) \, dS_j. \tag{10}$$

The above formulation accounts for all changes in fluxes through the control volume faces due to changes in their instantaneous positions. Since Reynolds' theorem is applied to the mesh rather than to a fluid volume, it is appropriate to designate this application as the 'mesh conservation law' by analogy with the geometric conservation law advocated by Thomas and Leonard.[13] The mesh conservation terms are automatically computed and incorporated into the numerical calculation to produce a true conservative formulation for the case of a moving mesh. This technique is only necessary for unsteady flow problems. In steady-state cases, there is no deformation of the control volume or displacement of the mesh. Also the application of this technique at every co-ordinate surface, $\xi_3 =$ constant, is equivalent to the application of the well known kinetic boundary conditions often used in open water modelling at the water surface level.

The velocity components ($\tilde{u}_i$) of the control volume in the Cartesian co-ordinates are calculated directly after the hydrodynamic properties of the flow. However, owing to the adopted definition of the co-ordinate transformation, $\tilde{u}_1$ and $\tilde{u}_2$ are functions of the horizontal movement of the water boundary, whereas $\tilde{u}_3$ is provided by the vertical movement of the free water surface. The component $\tilde{u}_3$ can be calculated as a fraction of the rate of change of water depth h at the concerned location.

Equation (9) can be written explicitly in the following form:

$$\left(\iiint_{V(\tau)} u_i \right)_\tau \Delta V + \sum_{m=1}^{6} \iint_{S_m(\tau)} \left[u_i u_j + \frac{P}{\rho} \delta_{ij} - u_i \tilde{u}_j - v_j (u_i)_j \right]_{S_m} \Delta S_{j(m)}, \quad i = 1,2, \quad j = 1,2,3, \tag{11}$$

with $\Delta S_{(m)} = (\Delta S_{j(m)}) = \Delta \xi_i \times \Delta \xi_k$.

The integration procedure of the finite volume formulation is extended to the continuity equation, where it is twice applied using a different control volume in each case. First, the continuity equation is integrated over a vertically adjacent column of control volumes covering the entire depth. This serves to obtain the equation used to calculate the water depth, which is

$$(h)_t + \sum_{\sigma=1}^{4} \left[\left(\int_{x_d^3}^{H} u_i \right)_i \right]_\sigma \mathrm{d}\sigma = 0, \quad i = 1,2. \tag{12}$$

Secondly, the continuity equation is integrated over a normal control volume to yield a recurrence equation that serves to calculate the Cartesian vertical component of the velocity, such as

$$[(u_1,u_2,u_3)\cdot\mathbf{dS}]_{n+1} = [(u_1,u_2,u_3)\cdot\mathbf{dS}]_n = -\left[\sum_{l=1}^{2} (u_1,u_2,u_3)\cdot\mathbf{dS} \right]_l - \left[\sum_{m=1}^{2} (u_1,u_2,u_3)\cdot\mathbf{dS} \right]_m. \tag{13}$$

The continuity equation itself is not verified explicitly during the computation process.

Initial and boundary conditions

A unique and convergent solution of the above set of equations requires the specification of initial and boundary conditions which complete the mathematical formulation of the problem.

Initial conditions may be prescribed as follows:

$$\begin{aligned} H(\xi_i) &= H_o = \text{constant}, \\ h(\xi_i) &= H_o(\xi_i) - x_d^3(\xi_1,\xi_2), \\ u_j(\xi_i) &= 0, \\ \rho(\xi_i) &= \rho_o = \text{constant}, \\ P(\xi_i) &= P_o(\xi_i) \text{ (local hydrostatic pressure)}. \end{aligned} \tag{14}$$

When more realistic field data are available, initial conditions may be set accordingly.

Boundary conditions are formulated, for reasons of generality, in terms of the contravariant (U^i) and covariant (U_i) components of the velocity at the fictitious cells of the boundary. At these cells the hydrodynamic properties are indexed by (o), whereas the insider cells are indexed by (i). Thus, a typical setting of the boundary conditions at $\xi_1 = C_1 = \text{constant}$ can be given as follows:

1. For slip boundary conditions (when assumed):

$$\begin{aligned} U^2_{(o)} &= -U^2_{(i)}, \\ U_{1(o)} &= U_{1(i)}. \end{aligned} \tag{15}$$

The corresponding Cartesian components of velocity can then be calculated by the following formula:

$$\begin{aligned} U_{1(o)} &= \frac{1}{\sqrt{g11}} \left[u_{1(i)} \left[\left(\frac{\partial x^1}{\partial \xi_1} \right)^2 - \left(\frac{\partial x^2}{\partial \xi_1} \right)^2 \right] + 2u_{2(i)} \frac{\partial x^1}{\partial \xi_1} \frac{\partial x^2}{\partial \xi_2} \right], \\ u_{2(o)} &= \frac{1}{\sqrt{g11}} \left[2u_{1(i)} \frac{\partial x^1}{\partial \xi_1} \frac{\partial x^2}{\partial \xi_2} + u_{2(i)} \left[\left(\frac{\partial x_2}{\partial \xi_1} \right)^2 - \left(\frac{\partial x^1}{\partial \xi_1} \right)^2 \right] \right]. \end{aligned} \tag{16}$$

Similar formulae are also used at other boundaries.

2. For non-slip boundary conditions simpler formulae may be applied, such as

$$U^i_{(o)} = -U^i_{(i)}, \quad j = 1,2,3, \tag{17}$$

or in terms of Cartesian components, it is simply

$$u_{j(o)} = -u_{j(i)}, \quad j = 1, 2, 3. \tag{18}$$

For other variables, such as ρ and h, the principle of reflection is applied.

At the free water surface, values of the shear stresses τ_{13} and τ_{23} are specified in terms of the first derivatives of velocity as

$$\begin{aligned} (\tau_{13}) &= \nu_1 (u_1)_3, \\ (\tau_{23}) &= \nu_2 (u_2)_3. \end{aligned} \tag{19}$$

The values of these stresses at the bottom of the flow are expressed in terms of the tangential components of velocity at the lower layer using a Manning-based quadratic approximation.

DISCRETIZATION PROCEDURE

The method used in this work to discretize the integral equations is based on an explicit second-order scheme, with its advantages of simplicity. Nevertheless, it must include some particular features relating to the problem of interpolating the values of various variables at cell faces. Also, the adaptation of an arbitrarily varying mesh, and the consistency of the algebraic end equations with the physical conservation laws must be well incorporated.

Variables associated with a volume integral are approximated by volumetric average values, whereas those associated with a surface integral are approximated by face average values. Thus, the corresponding finite difference operator of equation (11) can be written as follows:

$$\begin{aligned} &[u_i J]_c \Delta\xi_1 \Delta\xi_2 \Delta\xi_3 / \Delta\tau \\ &+ \left[u_i u_j + \frac{P}{\rho}\delta_{ij} - u_i \tilde{u}_j - \nu_j (u_i)_j \right]_w [(\xi^{1i}) \Delta\xi_2 \Delta\xi_3]_w \\ &- \left[u_i u_j + \frac{P}{\rho}\delta_{ij} - u_i \tilde{u}_j - \nu_j (u_i)_j \right]_e [(\xi^{1j}) \Delta\xi_2 \Delta\xi_3]_e \\ &+ \left[u_i u_j + \frac{P}{\rho}\delta_{ij} - u_i \tilde{u}_j - \nu_j (u_i)_j \right]_n [(\xi^{2j}) \Delta\xi_1 \Delta\xi_3]_n \\ &- \left[u_i u_j + \frac{P}{\rho}\delta_{ij} - u_i \tilde{u}_j - \nu_j (u_i)_j \right]_s [(\xi^{2j}) \Delta\xi_1 \Delta\xi_3]_s \\ &+ \left[u_i u_j + \frac{P}{\rho}\delta_{ij} - u_i \tilde{u}_j - \nu_j (u_i)_j \right]_{t_p} [(\xi^{3j}) \Delta\xi_1 \Delta\xi_2]_{t_p} \\ &- \left[u_i u_j + \frac{P}{\rho}\delta_{ij} - u_i \tilde{u}_j - \nu_j (u_i)_j \right]_b [(\xi^{3j}) \Delta\xi_1 \Delta\xi_2]_b = 0, \\ &\qquad i = 1, 2, \quad j = 1, 2, 3. \end{aligned} \tag{20}$$

The subscripts w, e, n, s, t_p and b correspond to the west, east, north, south, top and bottom faces of the control volume respectively; the subscript j indicates a repeated summation, J is the Jacobian of the transformation and (ξ^{1j}), (ξ^{2j}) and (ξ^{3j}) form the contravariant base vectors of the local curvilinear co-ordinate system, given by

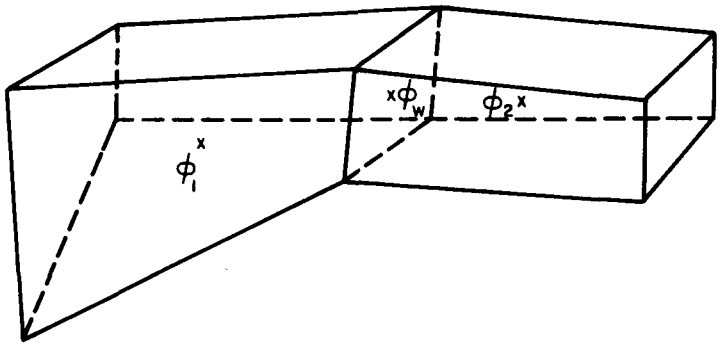

Figure 5. Simple linear approximation of $\phi_w = (Q_1 + Q_2)/2$ is clearly inadequate

$$\begin{aligned} \xi^1 &= (\xi^{1j}) = ((\xi_1)_1, (\xi_1)_2, 0), \\ \xi^2 &= (\xi^{2j}) = ((\xi_2)_1, (\xi_2)_2, 0), \\ \xi^3 &= (\xi^{3j}) = (0, 0, 1/h). \end{aligned} \tag{21}$$

The basic finite volume approach stipulates the use of the middle value interpolation $[(\phi_1 + \phi_2)/2$, for example] between adjacent cell values in order to calculate a corresponding face value. For instance, this second-order approximation may be suitable in the case of quasi-uniform and quasi-rectilinear meshes. But, in the case of a distorted or arbitrary mesh (Figure 5), this approximation is clearly unsuitable and should be replaced by a more accurate but still general approximation. Therefore, cell face values of the velocity components are expressed first in terms of the contravariant components of the velocity in the local curvilinear system. Then they are computed in terms of the Cartesian components of velocity. For example, the value of U^i at (e), the eastern wall of the control volume, is given by

$$[(U^i)]_l = \{[(U^i)]_{l-1,m,n} + [(U^i)]_{l,m,n}\}/2, \tag{22}$$

with

$$[(U^i)]_l = [(U^1, U^2, U^3)]_l$$

and

$$\begin{aligned} [U^1]_l &= [(\xi_1)_t + (\xi_1)_1 + (\xi_1)_2]_l, \\ [U^2]_l &= [(\xi_2)_t + (\xi_2)_1 + (\xi_2)_2]_l, \\ [U^3]_l &= [(\xi_3)_t + (\xi_3)_1 + (\xi_3)_2 + (\xi_3)_3]_l. \end{aligned}$$

The idea is that the contravariant components of the velocity hold in their definition the geometric characteristics of the local co-ordinate system (or the grid). These are related to metric dimensions, orientations and deformations. Moreover, these velocity components can be interpreted as weighted projections of the velocity in the directions of their respective contravariant base vectors. These vectors are alternatively perpendicular to their opposite covariant base vectors, which constitute the local control volume boundaries. However, this physically sound approximation induces some complexity into the formulation that requires additional computing time. The Cartesian components of the velocity can then be given by

$$[(u_i)]_e = [G^{-1}](U^i - (\xi_i)_t)]_e, \tag{23}$$

where G^{-1} is the inverse metric matrix, expressed as

$$[G^{-1}] = \frac{1}{J}\begin{bmatrix} (\xi_2)_2 & (\xi_3)_3 & -(\xi_1)_2 & (\xi_3)_3 & 0 \\ -(\xi_2)_1 & (\xi_3)_3 & (\xi_1)_1 & (\xi_3)_2 & 0 \\ (\xi_2)_1 & (\xi_3)_2 - (\xi_2)_2 & (\xi_3)_1 (\xi_1)_2 & (\xi_3)_1 & -(\xi_1)(\xi_3)_2 (\xi_1)_1 (\xi_2)_2 - (\xi_1)_2 (\xi_2)_1 \end{bmatrix} \tag{24}$$

Similar formulae ought to be used at each of the control volume faces.

The discretized equation yielding the Cartesian components of velocity at the centre of the computational cell in terms of the curvilinear coordinates is given by

$$\begin{aligned}
[u_i h]_c^{n+1} = [u_i h]_c^n
&- \frac{\Delta\tau}{[(\xi_1)_1(\xi_1)_2 - (\xi_1)_2(\xi_2)_1]} \Bigg\{ \frac{1}{\Delta\xi_1} [[u_i u_1 - u_i \tilde{u}_1 - (v_1 u_i)_1]_w [(\xi_1)_1]_w \\
&+ [u_i u_2 - u_i \tilde{u}_2 - (v_2 u_i)_2]_w [(\xi_1)_2]_w \\
&- [u_i u_1 - u_i \tilde{u}_1 - (v_1 u_i)_1]_e [(\xi_1)_1]_e \\
&- [u_i u_2 - u_i \tilde{u}_2 - (v_2 u_i)_2]_e [(\xi_1)_2]_e] \\
&+ \frac{1}{\Delta\xi_2} [[u_i u_1 - u_i \tilde{u}_1 - (v_1 u_i)_1]_n [(\xi_2)_1]_n \\
&+ [u_i u_2 - u_i \tilde{u}_2 - (v_2 u_i)_2]_n [(\xi_2)_2]_n \\
&- [u_i u_1 - u_i \tilde{u}_1 - (v_1 u_i)_1]_s [(\xi_2)_1]_s \\
&- [u_i u_2 - u_i \tilde{u}_2 - (v_2 u_i)_2]_s [(\xi_2)_2]_s] \\
&+ \frac{1}{\Delta\xi_3} [[u_i u_1 - u_i \tilde{u}_1 - [(v_1 u_i)_1]_{t_p} [(\xi_3)_1]_{t_p} \\
&+ [u_i u_2 - u_i \tilde{u}_2 - (v_2 u_i)_2]_{t_p} [(\xi_3)_2]_{t_p} \\
&+ [u_i u_3 - u_i \tilde{u}_3 - (v_3 u_i)_3]_{t_p} [(\xi_3)_3]_{t_p} \\
&- [u_i u_1 - u_i \tilde{u}_1 - (v_1 u_i)_1]_b [(\xi_3)_1]_b \\
&- [u_i u_2 - u_i \tilde{u}_2 - (v_2 u_i)_2]_b [(\xi_3)_2]_b \\
&- [u_i u_3 - u_i \tilde{u}_3 - (v_3 u_i)_3]_b [(\xi_3)_3]_b] + \Pi_i \Bigg\}^n, \quad i = 1, 2,
\end{aligned} \tag{25}$$

with

$$\begin{aligned}
(\xi_1)_1 &= (x^2_{\xi_2} \alpha h) J^{-1}, \\
(\xi_1)_2 &= -(x^1_{\xi_2} \alpha h) J^{-1}, \\
(\xi_1)_3 &= 0, \\
(\xi_2)_1 &= -(x^2_{\xi_1} \alpha h) J^{-1}, \\
(\xi_2)_2 &= (x^1_{\xi_1} \alpha h) J^{-1}, \\
(\xi_2)_3 &= 0, \\
(\xi_3)_1 &= (x^2_{\xi_1} x^3_{\xi_2} - x^3_{\xi_1} x^2_{\xi_2}) J^{-1}, \\
(\xi_3)_2 &= (x^1_{\xi_2} x^3_{\xi_1} - x^1_{\xi_1} x^3_{\xi_2}) J^{-1},
\end{aligned} \tag{26}$$

$$(\xi_3)_2 = (x^1_{\xi_1} x^2_{\xi_2} - x^1_{\xi_1} x^2_{\xi_1}) J^{-1}$$

and

$$\begin{aligned}\Pi_i = \frac{J^{-1}}{\rho}\Big\{ & [\alpha P h]_w [\delta_{i1} x^2_{\xi_2} - \delta_{i2} x^1_{\xi_2}]_w \\ & - [\alpha P h]_e [\delta_{i1} x^2_{\xi_2} - \delta_{i1}{}^2 x^1_{\xi_2}]_e \\ & + [\alpha P h]_n [\delta_{i_1} x^1_{\xi_1} - \delta_{i_2} x_{\xi_1}]_n \\ & - [\alpha P h]_s [\delta_{i1} x^1_{\xi_1} - \delta_{i2} x^2_{\xi_1}]_s \\ & + [P]_{t_p} [[x^2_{\xi_1} x^3_{\xi_2} - x^3_{\xi_1} x^2_{\xi_2}]_{t_p} \delta_{i1}] \\ & + [x^1_{\xi_2} x^3_{\xi_1} - x^1_{\xi_1} x^3_{\xi_2}]_{t_p} \delta_{i2}] \\ & - [P]_b [[x^2_{\xi_1} x^3_{\xi_2} - x^3_{\xi_1} x^2_{\xi_2}]_b \delta_{i1}] \\ & + [x^1_{\xi_2} x^3_{\xi_1} - x^1_{\xi_1} x^4_{\xi_2}]_b \delta_{i2}]\Big\}, \quad i = 1, 2. \end{aligned} \tag{27}$$

Pressure approximation

The use of the hydrostatic approximation yields the following formula for the pressure P:

$$P = P_s + \rho g_r (h + x^3_d - x^3), \tag{28}$$

where P_s is the atmospheric pressure at the level of the water surface.

The incorporation of this formula into the integral equations results in a quadratic term of h. The linear interpolation of the h^2 terms renders the difference equations inconsistent with the basic conservation laws. A simple remedy for each quadratic term and each volume face would only be practically unfeasible. In fact, we devise here a macro approximation based on overall balance of pressure forces for the computational cell under zero-flow condition (Figure 6). This implicitly uses a different pressure approximation at each face of the control volume ensuring the consistency requirement as follows (in the ξ_1 direction):

$$\begin{aligned}\Pi_1 = & - g_r h^2_w \Delta\xi_3 (1 - \xi_{3b}) \Delta x^2_{\xi_{2w}} \\ & + g_r h^2_e \Delta\xi_3 (1 - \xi_{3b}) \Delta x^2_{\xi_{2w}} \\ & + g_r \frac{(h_e + h_w)}{2} [(h_e - h_w)\xi_{3b} + (x^3_{d_e} x^3_{d_w})](1 - \xi_{3b}) \Delta x^2_{\xi_{2w}} \\ & - g_r \frac{(h_e + h_w)}{2} [(h_e - h_w)\xi_{3t_p} + (x^3_{d_e} - x^3_{d_e})](1 - \xi_{3t_p}) \Delta x^2_{\xi_{2w}} \\ & + g_r h^2_s \Delta\xi_3 (1 - \xi_{3b}) \Delta x^2_{\xi_{1s}} \\ & - g_r h^2_n \Delta\xi_3 (1 - \xi_{3b}) \Delta x^2_{\xi_{1s}} \\ & - g_r \frac{(h_n + h_s)}{2} [(h_n - h_s)\xi_{3b} + (x^3_{d_n} - x^3_{d_s})](1 - \xi_{3b}) \Delta x^2_{\xi_{1s}} \\ & + g_r \frac{(h_n + h_s)}{2} [(h_n - h_s)\xi_{3t_p} + (x^3_{d_n} - x^3_{d_s})](1 - \xi_{3t_p}) \Delta x^2_{\xi_{1s}}. \end{aligned} \tag{29}$$

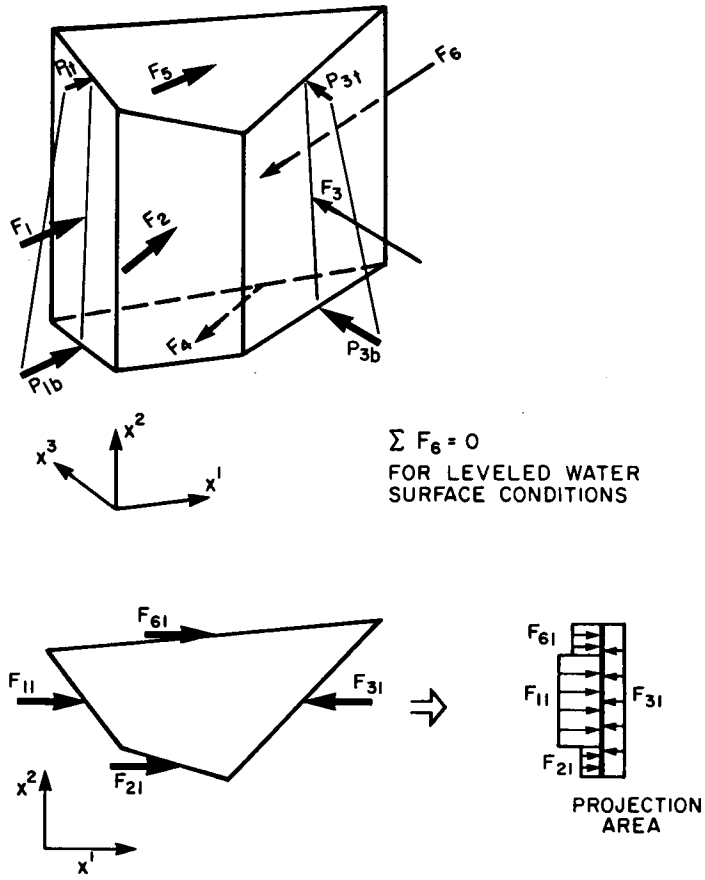

Figure 6. Pressure balance over a control volume for a levelled water surface condition

The metrics present in the above equation, as well as in the momentum equations, are calculated on the basis of a first-order approximation, such as

$$x^i_{\xi_j} = \frac{[x^i]_{l+1,m,n} - [x^i]_{l,m,n}}{[\Delta\xi_j]_{l,m,n}}. \tag{30}$$

STABILITY REQUIREMENT AND COMPUTATIONAL ALGORITHM

In surface water flow simulations, convective terms are mostly dominant whereas diffusion terms averaged over normally long distances are less significant. Therefore, the positive effect of the diffusive terms, as a stabilizing factor, is greatly lessened. This leaves any generated oscillation growing uncontrollably and threatens the capability of a central difference scheme to produce a stable and convergent solution. In order to rectify this problem it was thought opportune to adopt an artificial viscosity damping factor. This is applied only in the two-dimensional planar direction. With the exception of having specially defined variable coefficients, the following is based on a similar correction given by Gnoffo:[14]

$$[u_i]_c^{n+1} = [u_i]_c^{n+1} + C_S[u_i]_S^{n+1} + C_N[u_i]_N^{n+1}$$

$$+ C_W[u_i]_W^{n+1} + C_E[u_i]_E^{n+1}, \quad i = 1,2. \tag{31}$$

C_S, C_N, C_W and C_E are set as functions of the local water surface gradient in the planar direction. The proportionality factors are estimated in the order of the corresponding local $(1/\Delta\xi_i)$ metric.

The calculation algorithm is performed according to the following steps:

1. Identify the initial position of the physical boundaries and the initial water surface elevations.
2. Generate the initial grid system and calculate the corresponding metrics.
3. Compute u_1 and u_2 using equation (25) but without Π_i.
4. Calculate u_3 and the water depth h.
5. Recalculate u_1 and u_2 by applying Π_i.
6. Correct u_1 and u_2 by using equation (31).
7. Redefine the position of the grid elements and update the metric values.
8. Go to 3.

TESTS AND RESULTS

Several computational tests have been performed to verify the capability of the model in achieving stability, convergence, and accuracy in a number of typical open water problems. Although the algorithm is devised for general three-dimensional flow with irregular geometry and bathymetry, it can obviously be applied to regular rectangular geometry problems. These are needed to test some of the characteristics of the model, such as symmetry, diffusivity and ability to approximate simple analytical solutions or to match available results from published materials.

The first application of the model was to test its consistency with the physical situation and its ability to conserve the state of zero flow or reproduce interchangeably a constant or equally varied velocity distribution. In the zero-flow test, the initial boundary conditions consisted of a zero slope in the free water surface as well as a zero velocity field. A variant slope in the bottom of the basin was introduced, rendering the test meaningful and providing the possibility of having unequal pressure forces at each of the control volume faces. In this case, the momentum equation is reduced to Π_i only. The Π_i approximation given by equation (29) assured a successful and perfect zero velocity for an undetermined period of calculation. Another basic test consisted of measuring the model adequacy in conserving the hydraulic properties of the movement of a propagation wave having an amplitude of 2 m and a period of 50 s in a 5 m deep and 100 m long basin. The calculation showed a perfect reproduction of the wave period and a synchronization of the amplitude with an invariable factor of dissipation.

Oscillation of a standing wave in a closed basin

This example is intended to simulate the hydrodynamic behaviour of the repetitive motion of a stationary wave and to examine the effects of the deformability of the grid system in the vertical direction on the stability of the scheme and the authenticity of the results. The basin considered was 100 m long, 50 m wide and 5 m deep. The dimensions of the grid systems used were ($10 \times 5 \times 5$) and ($20 \times 10 \times 5$), respectively. These allowed the determination of the effect of mesh refinement of the behaviour of the solution. A small mesh dimension and a reduced basin size are intended to test the effects of non-linear terms and their influence on the stability of the numerical scheme.

As initial conditions a sinusoidal free water surface profile was imposed at time $t = 0$. This produced a maximum depth of 6 m at the left end of the basin and a minimum depth of 4 m at the right end. The potential energy stored in the initial standing wave will suddenly be released and

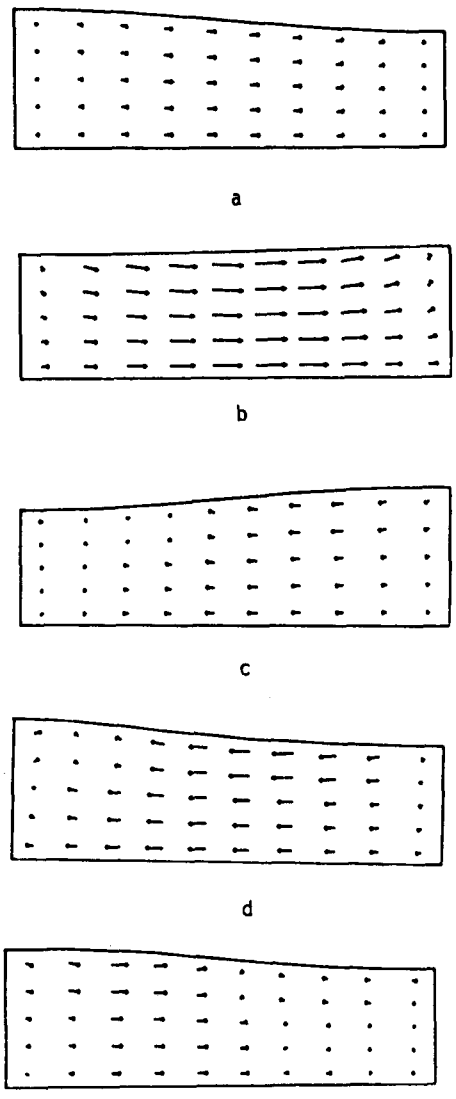

Figure 7. Sequences of flow free movement—vertical view, $\Delta t = 0{\cdot}5$ s, $\nu = 0{\cdot}05$ m^2/s: (a) $t = 10$ s, (b) $t = 35$ s, (c) $t = 70$ s, (d) $t = 125$ s, (e) $t = 155$ s

transformed into a repetitive back and forth movement at the natural resonance period of the basin. Slip boundary conditions were used in order to alleviate the retardment factors and to be able to compare the results with Reference 8 and the linear wave theory. In Reference 8, Leendertse *et al.* used a far larger basin and completely removed the advective non-linear terms of the equation, which are the most significant factors in such problems, affecting the stability of the numerical scheme.

Figure 7 illustrates the various sequences of the movement of this suddenly generated wave in a vertical plane. The reversible and oscillatory characteristics of the movement produce and preserve approximately the same value of the period $T = L/\sqrt{(gh)}$ of a gravity wave having an average water

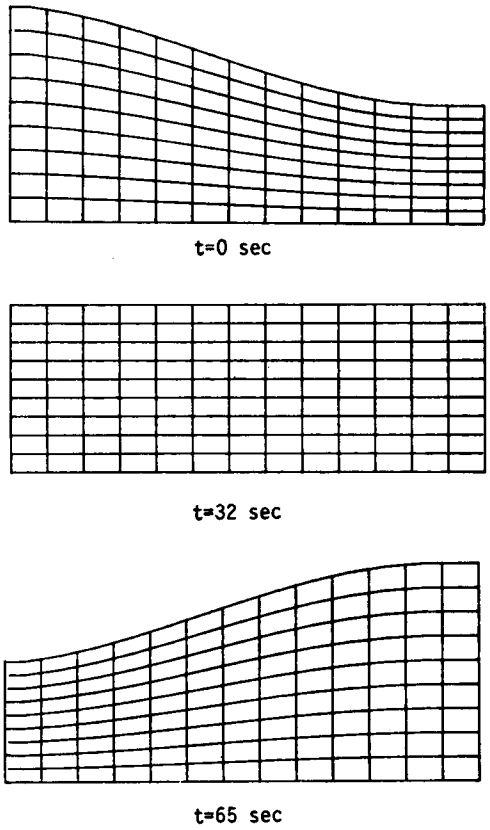

Figure 8. Mesh adaptation to the reversal movement of the free water surface

depth $h = 5$ m and a propagating celerity $= \sqrt{(gh)}$. L is the length of the basin. Figure 8 illustrates the oscillatory movement of the mesh that follows at all times the configuration of the free water surface. The vertical component of the intrinsic velocity of a control volume in the flow field changes sign during the computation of the reversal current in complete harmony with the overall movement of water.

The histories of the water surface level location (h) and of the longitudinal velocity component (u) near the end and at the centre of the basin are shown in Figures 9 and 10, respectively. The non-linear term effects are more appreciable at the centre than at the end of the basin. Even though the undulatory form of the variations of (h) or (u) departs from ideal harmony, especially after the first reversal, it conserves approximately the same period (T) value at both locations.

Wind driven circulation

This test described the transient response of the model to a sudden wind shear stress corresponding to a wind speed of 40 km/h applied at the free water surface. Initially, the water was at rest, velocity was set to zero everywhere with a horizontal water surface profile. The test basin had a rectangular shape 2600 m long, 1200 m wide and 7 m deep. It was arbitrarily fitted with a ($13 \times 12 \times 7$) node grid where $\Delta\xi = 200$ m, $\Delta\eta = 100$ m and $\Delta\zeta = 1$ m. The time step was fixed at a 5 s increment. The wind was maintained at a constant speed up to the 255th time step

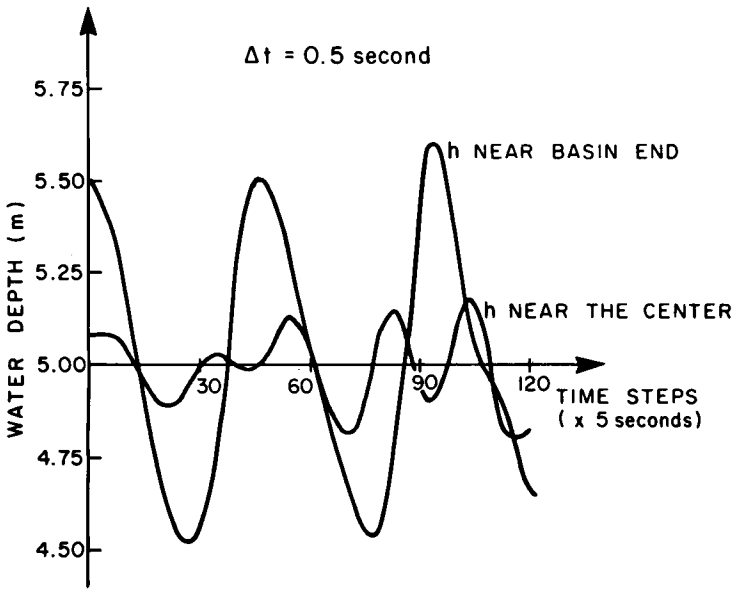

Figure 9. Variation of the free surface level at the centre and of the basin

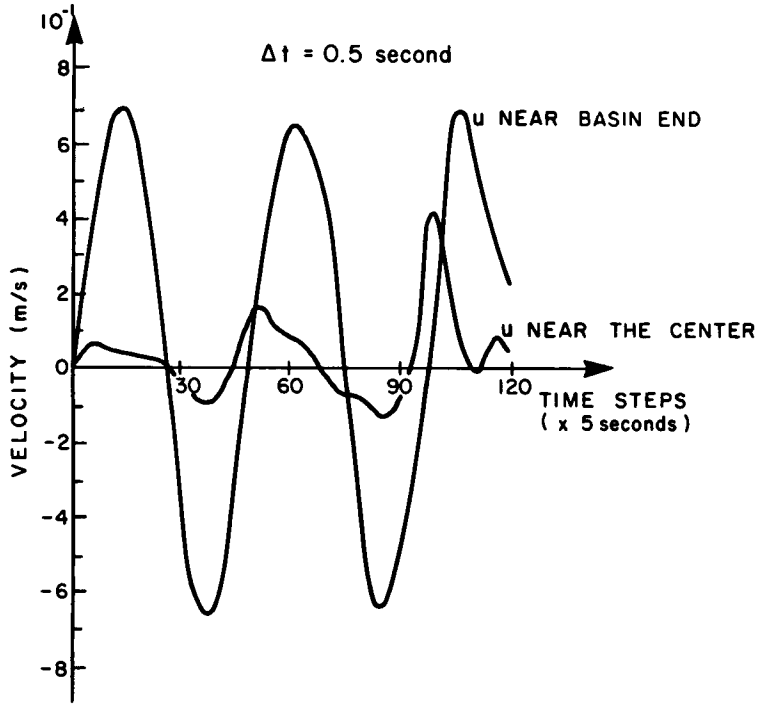

Figure 10. Variation of the horizontal component of velocity at the centre and the end of the basin

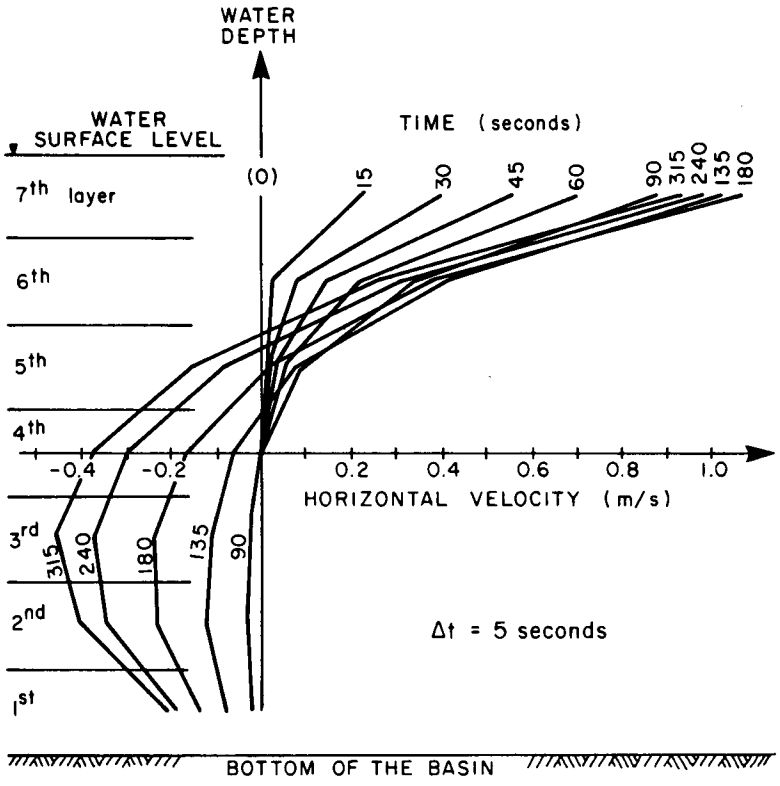

Figure 11. The evolution of the velocity profile over the water depth at the basin centre

when it was suddenly stopped and the water movement was left to alternate freely.

Figure 11 shows the evolution of the velocity profile along the depth of the water at the basin centre. This series of curves represents the velocity profiles at different time intervals, starting from the initial moment up to 315 s, at which point subsequent velocity profiles oscillate moderately. These oscillations are apparent in Figure 12, where they are compared with rather more abrupt and sudden ones produced in the Reference 8 model. The oscillations are a result of the transient response of the water body to the sudden application of wind stress at the water surface. Their pattern is greatly influenced by the continual and rather complex interaction between the non-linear convective terms and the viscous terms excited by this sudden imposition of stress at the water surface. Figure 12 shows also the history of the development of the longitudinal component (u) of velocity at each of the seven layers covering the water depth.

The comparison with Reference 8 results is a good indication of the improved stability provided by the special formulation of the finite volume approach presented in this work.

The velocity field is shown in Figure 13 in a sequence of projections on a vertical plane covering the duration of computation at certain intervals in time. They show the gradual development of the circulation, first in the upper layers and thereafter in the bottom layers, with a reversal in current. This circulation is the product of vertical momentum transfer.

Viscous coupling and debalancing in the water surface is due to wind push-up at the frontal end of the basin. The latter can be viewed as the accumulation of potential energy responsible for the continuation of the circulation and the oscillation in the velocity profile in Figure 13 after the wind has been stopped.

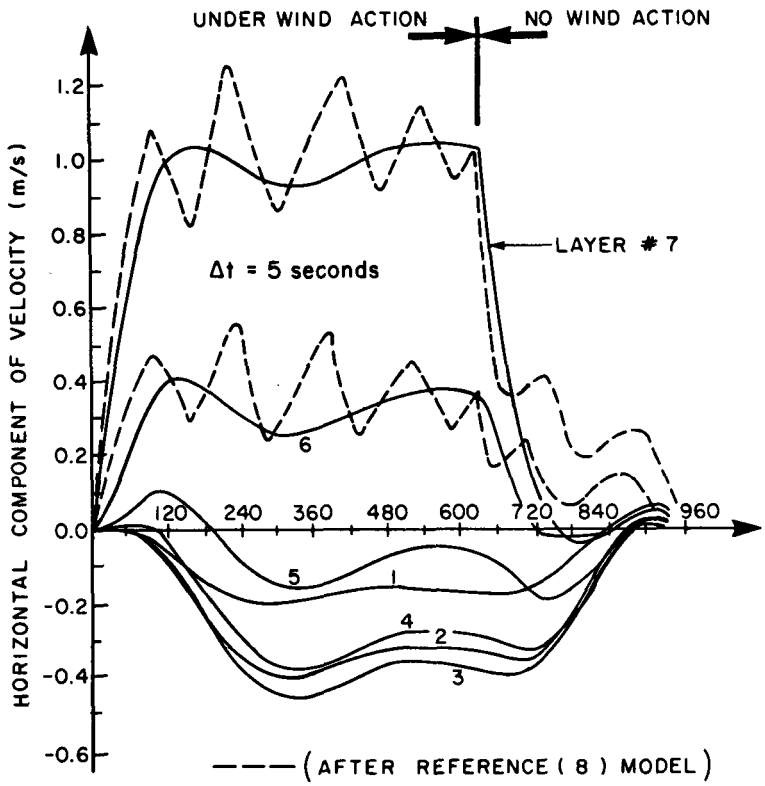

Figure 12. Temporal variation of the velocity at each layer throughout the depth

Flow in a strongly curved channel

The flow of water in a channel bend is characterized by its complex three-dimensional pattern due to the generation of a transverse helicoidal circulation and the displacement of the centre of motion from one side to another across the bend. In addition, at a relatively high velocity, separation of flow may occur. The following test deals with the simulation of flow behaviour in a stable but strongly curved channel.

A strongly curved channel is generally characterized by having a small radius to width ratio ($r_0/B \leqslant 3$; r_0 is the radius of the channel centre-line and B is the channel width). In the present case this ratio is taken to be equal to 1·5, with $r_0 = 60$cm and $B = 40$cm. The simulation results are compared with experimental data given by Goncharov;[15] yet there exist no analytical solutions of such problems. However, some attempts were made to derive analytical solutions for weakly curved flow but not without a broad range of assumptions, such as axisymmetric and potential flow conditions.[15,16]

The channel curve consists of a 135° bend with extended straight inlet and outlet reaches of length $L = B =$ channel width. The water depth is taken equal to 6cm, as given in Reference 15. The longitudinal profile of the velocity at the inlet is set according to the experimental data with an average value of 0·26m/s. The vertical profiles are assumed to follow the 1/7th power law. The Reynolds number $N_R = V_{\xi_2} h/v$ is equal to 15,540 and the Froude number $F = V_{\xi_2}/\sqrt{(g_r h)} = 0{\cdot}338$.

Three-dimensional views of the grid system are shown in Figure 14. These give the configuration of the mesh used at the starting time, where a constant water depth was assumed, and at the

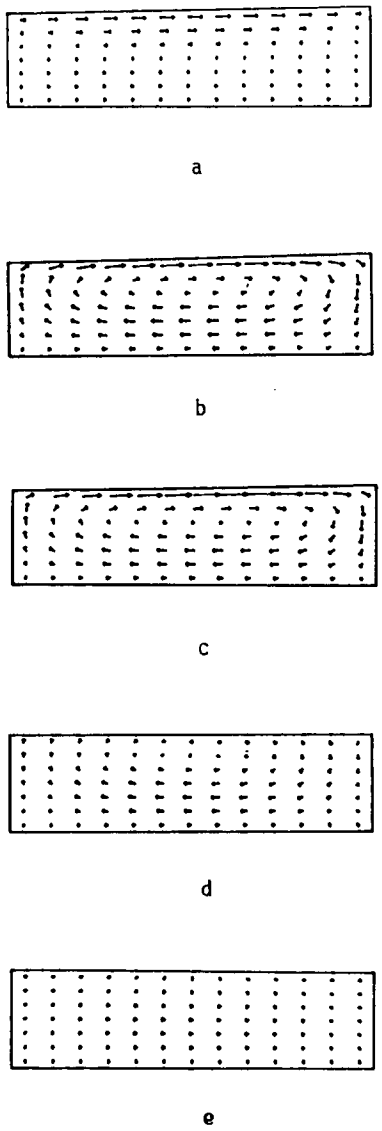

Figure 13. Sequences of flow pattern—vertical view, $\Delta t = 5$ s, $v = 0{\cdot}01$ m^2/s: (a) $t = 50$ s, (b) $t = 900$ s, (c) $t = 2100$ s, (d) $t = 3500$ s, (e) $t = 4500$ s

10,000th time step after the steady-state condition was established. The calculated water surface elevation is plotted in contour line form in Figure 15. It reveals a transverse surface slope with a maximum inclination of about 6 mm which occurs at an angle of about 35° from the beginning of the bend. Reference 15 reported maximum inclination at about a 36° angle. The calculation shows an average of 1·8 mm in difference between the inlet and the outlet water surface levels compared to 2 mm reported for the experimental results.

Figure 16 shows the depth-averaged velocity profiles in the radial direction at various sections along the bend. Figure 17 gives a comparison between the experimental data, given as dashed lines, and the calculated profile, plotted as continuous lines. The agreement between the curves is quite

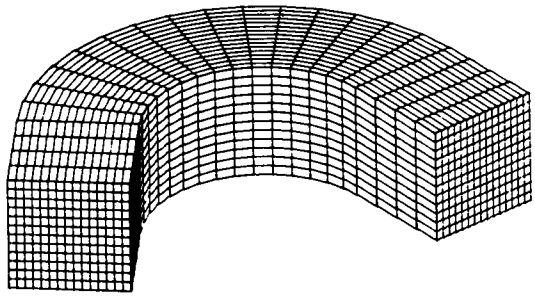

(a)

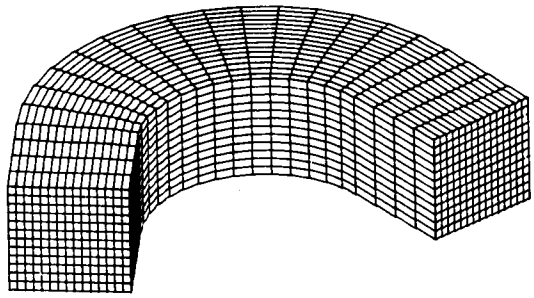

(b)

Figure 14. Three-dimensional view of the evolving mesh: (a) initial mesh; (b) final mesh (steady state)

satisfactory, and the predicted curves reproduce to a good degree the overall behaviour of the flow velocity. The transitional variations of the velocity profile along the bend are due to the fact that the fluid mass tends to resist the channel curvature and the liquid particles tend to cross the bend with no rotation. The discrepancy between the experimental and predicted values shows a tendency slightly to increase towards the outlet zone of the bend. On the other hand, a much larger discrepancy (Figure 18) was found between the calculated and measured values of radial transverse velocity components, which are generally of much lower order than the longitudinal velocity components. It should be noted that the use of the hydrostatic pressure assumption and the neglect of the vertical acceleration have a retarding effect on the full establishment of the circulation, especially in the present case where the water depth was set to 0·06 m.

CONCLUSION

A computational model has been presented for the simulation of general three-dimensional free-surface flow. The model is based on a conservative finite volume approach for the solution of the three-dimensional equation of continuity and momentum components. Important features of the formulation include the use of a time-dependent mesh adaptive system that continuously fits the

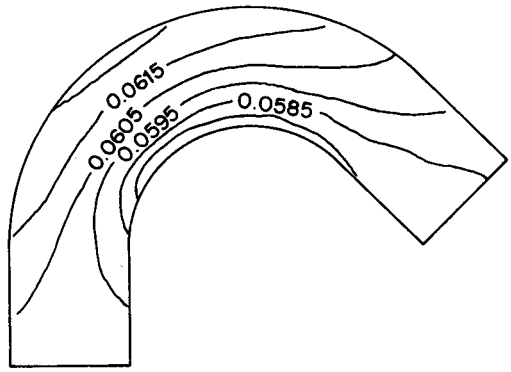

(a)

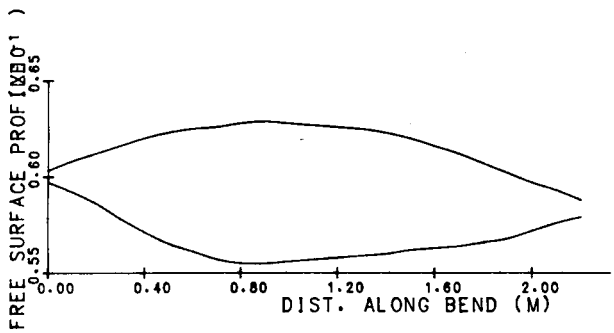

(b)

Figure 15. (a) Water surface elevation shown in contour lines. (b) Water elevations at the inner and outer boundaries of the bend

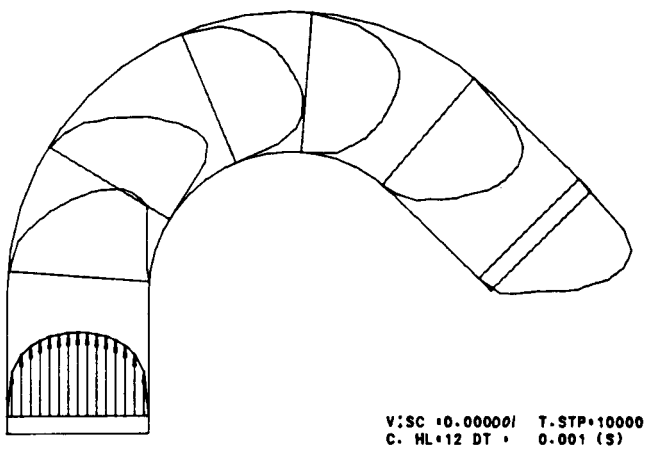

Figure 16. Longitudinal velocity profiles (V_{ξ_2}/V_A) at various sections in the bend (V_A is the depth-averaged velocity)

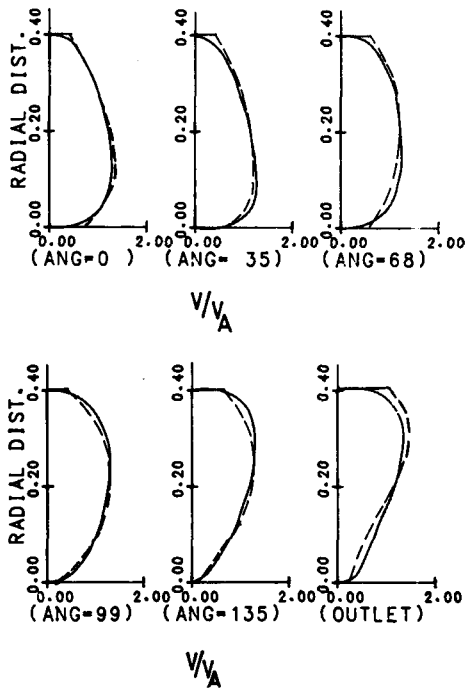

Figure 17. Comparison between calculated and measured longitudinal velocity profiles (V_{ξ_2}/V_A) (V_A is the depth-averaged velocity): ——— calculated profile; ----- measured profile

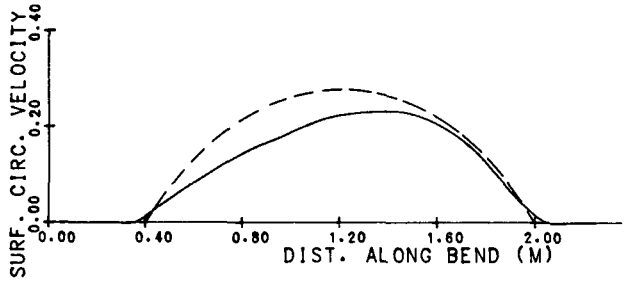

Figure 18. Comparison between calculated and measured radial velocity profile (V_{ξ_2}/V_A) at the centre of the bend: ——— calculated profile; ----- measured profile

boundaries including the moveable free water surface. The model has been applied in a series of different flow situations peculiar to open water flow problems. The predictive capability of the model, especially in the case of wind-driven circulation and the flow around a channel bend, is rated as satisfactory, and would allow the addition of a turbulent model to simulate more complex flow situations.

ACKNOWLEDGEMENTS

The calculations of the various cases in this paper were performed on the IBM 3480 computer of the Ecole polytechnique de Montréal. The authors wish to acknowledge the NSERC research funds for the research grant under which this work was carried out.

REFERENCES

1. B. P. Leonard, 'A stable and accurate convective modelling procedure based on quadratic upstream interpolation', *Computer Methods in Applied Mechanics and Engineering*, **19**, 59–98 (1979).
2. W. G. Gray, 'Do finite element models simulate surface flow?', in J. D. Wang *et al.* (eds), *Finite Elements in Water Resources*, University of Mississippi, 1978, 1.122–135.
3. A. F. Blumberg, 'Numerical tidal model of Chesapeake Bay', *Hydraulics Div., ASCE*, **103**, 1–10 (1977).
4. J. J. Leendertse, 'A water quality simulation model for well-mixed estuaries and coastal seas', *Rand Corp. Memo*, Vol. 1, RM-6230-RC, 1970.
5. S. W. Bauer and K. D. Schmidt, 'Irregular-grid finite-difference simulation of Lake Geneva surge', *J. Hydraulic Engineering*, **109**, 1285–1297 (1983).
6. H. G. Ramming, 'A nested North Sea model with fine resolution in shallow coastal rivers', *Proc. Soc. Roy. Sc. Liège, Series 6*, **10**, 9–26 (1976).
7. J. P. Benqué, J. A. Cunge, J. Feuillet, A. Haunguel and F. M. Holly, 'New method for tidal current computation', *J. Water, Port, Coastal and Ocean Div., ASCE*, **108**, 396–417 (1982).
8. J. J. Leendertse, R. C. Alexender and S. K. Liu, 'A three-dimensional model for estuaries and coastal seas', *Rand Corp. Rep.*, Vol. I, No. R-1417-OWRR, 1973.
9. S. Sengupta, H. P. Miller and S. S. Lee, 'Effect of open boundary conditions on numerical simulation of three-dimensional hydrothermal behavior of Biscayne Bay, Florida', *Int. j. numer. methods Fluids*, **1**, 145–169 (1981).
10. B. P. Leonard, M. A. Leschziner and J. McGuirk. 'Third-order finite-difference method for steady two-dimensional convection', *Proc. Int. Conf. on Num. Meth. in Laminar and Turbulent Flow*, 1978, pp. 807–819.
11. R. Chapman, and C. Y. Kuo, 'Application of a high accuracy finite difference technique to steady, free surface flow problems', *Int. j. numer. methods Fluids*, **3**, 583–590 (1983).
12. J. F. Thompson, F. C. Thames and W. Mastin, 'Automatic numerical generation of body-fitted curvilinear coordinate system for field containing any number of arbitrary 2-D bodies, *J. Comp. Phys.*, **15**, 219–319 (1974).
13. P. D. Thomas and C. K. Leonard, 'Geometric conservation law and its application to flow computation on moving grid', *AIAA, J.*, **17**(10), 1030–1037 (1979).
14. P. A. Gnoffo, 'Solutions of the Navier–Stokes equations for supersonic flow over blunt bodies in a generalized orthogonal coordinate system', *M. S. Thesis*, Polytechnic Institute of Brooklyn, 1974.
15. V. N. Goncharov, *Dynamics of Channel Flow*, Israel Program for Scientific Translation, Jerusalem, 1964.
16. B. C. Yen, 'Characteristics of subcritical flow in a meandering channel', Institute of Hydraulic Research, University of Iowa, 1965.